Modularized, Reconfigurable and Bidirectional Charging Infrastructure for Electric Vehicles with Silicon Carbide Power Electronics (MoReSiC)

Deliverable D6.1 (Month 39)

Title: "Complete integrated EV charging system with 20 kVA multilevel AC-DC converter, two 10/20 kW isolated DC-DC converters and 20 kW non-isolated DC-DC converters under control of the power flow controller"

Authors: Authors: Krzysztof Kalinowski, Rafał Miśkiewicz, Michał Harasimczuk, Grzegorz Wrona, Przemysław Trochimiuk, Rafał Kopacz, Jacek Rąbkowski, Warsaw University of Technology; Kaushik Naresh Kumar, Dimosthenis Peftitsis, NTNU; Radosław Sobieski, Markel;

Executive summary

The deliverable includes the description of the whole advanced electric vehicle charging system, including the grid converter, battery energy storage converter, EV interfacing isolated dc-dc converters, and the converter dedicated to photovoltaic inclusion. Apart from the basic description of the built experimental setup, the results are also exhibited, successfully validating the system and the energy management algorithm from D1 in several possible operation modes.

Table of Contents

1. Description of the vehicle charging system with additional non-isolated DC/DC converter interfacing PV plant

Initially, the whole advanced electric vehicle (EV) charging system consisted of three types of bidirectional power electronics converters: a three-level active rectifier with a three-port DC output to interface with a 3-phase grid, non-isolated three-level DC/DC converter interfacing energy storage (ES) and isolated DC/DC converters interfacing EVs. However, according to Annex MoReSiC-UA titled "Photovoltaic Extension for Bidirectional Charging Infrastructure for Electric Vehicles," the system was enhanced by a unidirectional, three-level, non-isolated DC/DC converter. The additional converter was responsible for delivering energy from a renewable energy source – photovoltaic (PV) plant – to the charging system, which enriched the possibility of island operation of the system and should decrease the total cost of energy supplied from the grid. The maximum power delivered by this converter is equal to 10 kW. The block diagram of the enhanced advanced EV charging system is presented in Figure 1. Obviously, the inclusion of the additional converter leads to more possible operating modes. However, their description of the proposed power flow controller is covered in the report Deliverable D1.1.

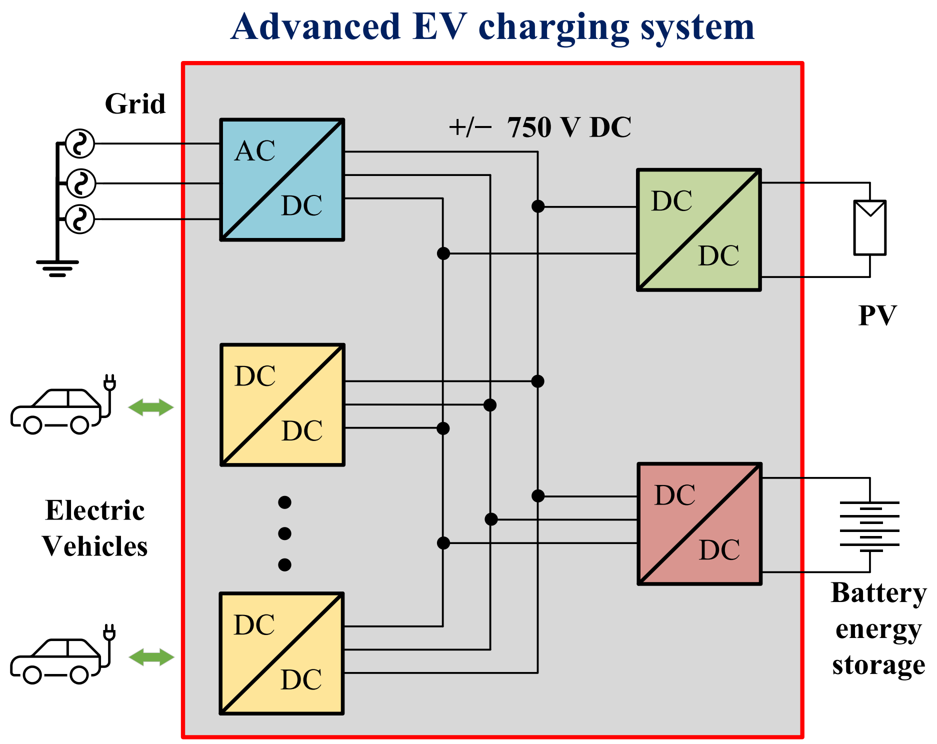

Fig. 1 Scheme of the advanced EV charging system enhanced with additional PV plant DC/DC converter.

2. Description of the non-isolated DC/DC converter interfacing PV plant with advanced EV charging system

The simplest way to increase the share of renewable energy delivered to EVs or ES is to connect the PV plant (through a DC/DC converter), which may be built in the neighborhood of the EV charging station, to the system. The output of the converter interfacing PV plant should be connected to the DC terminals, which couples all converters in the system. However, the choice of topology and design stage of such a solution are not straightforward, especially when certain requirements are imposed in advance by the previously built system. Thus, in the following sections, the selection of proper topology, converter control algorithm, simulation tests, as well as the design of the prototype and its experimental verification are included.

2.1 Topology

To select the topology of the DC/DC converter interfacing PV plant with the DC-link of the EV charging system, some constraints and requirements have been analyzed. First, the possible output voltage span of PV (V_{PV}) from 300 V to 800 V was assumed, which is a common value for PV plants. Thus, considering the nominal V_{DC} voltage in the system (1.5 kV), the chosen topology has to have a voltage step-up characteristic. The maximum power of the mentioned converter was established at 10 kW. As the energy flows only from the PV plant to the station, a unidirectional topology is sufficient. Moreover, there are no isolation requirements for PV applications. Hence, a non-isolated converter could be implemented. Finally, the chosen topology should be able to match the designed submodule (see Deliverable D2.1), which is the basis on which each converter in the system is built. Taking into consideration the abovementioned conditions, as well as the researched possibility to limit the station-side current ripples in certain operating modes, the flying capacitor (FC) leg was selected to build the unidirectional, three-level, non-isolated DC/DC converter interfacing PV plant with previously built advanced EV charging system. Such topology fulfills all listed requirements and enables to convert DC energy in a medium voltage range with high efficiency. Moreover, to reduce the ripples of current drawn from the PV plant, an interleaved structure consisting of two legs – Leg A and Leg B – was applied. The complete schematic of the selected topology is depicted in Figure 2.

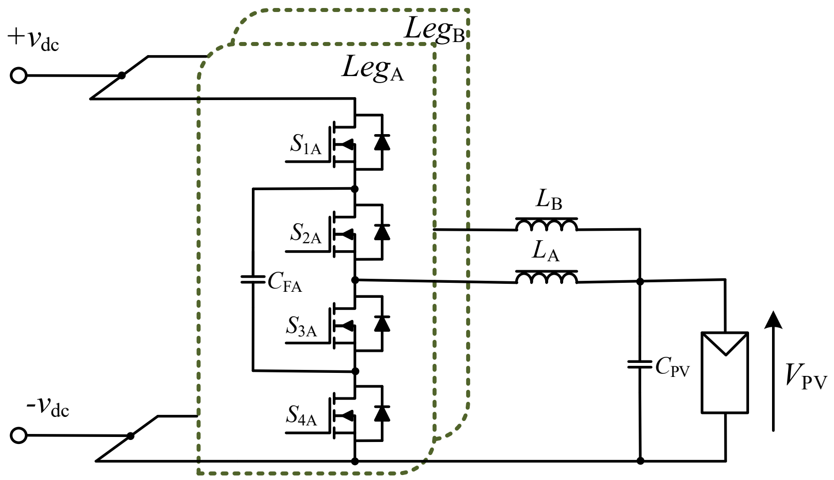

Fig. 2 Scheme of the interleaved FC converter, interfacing PV plant and the EV charging system.

2.2 Control algorithm

In the next step, the control algorithm was developed to ensure proper operation of the selected topology with the rest of the system in different operating modes. The schematic of the adopted control strategy is depicted in Figure 3. The control algorithm calculates the proper control signals for $S_{1A}\div S_{4A}$ and $S_{1B}\div S_{4B}$ transistors based on two control loops. The main loop decides on the power flow according to MPPT (maximum power point tracking) module to maximize the power drawn from the PV plant. The loop consists of a PV-side voltage PI (proportional-integral) controller fed by the MPPT module, which then outputs inductor current reference values i_{Lref} based on the properties of the PV plant and measured PV-side voltage V_{PV}. Note that as there are two legs, the reference current is divided by 2. Further, the reference value is compared with the measured value of the current and fed to the current PI controller, which finally results in a duty cycle d for the transistors. Apart from the main loop, there is a secondary loop for flying capacitor voltage balancing, which is necessary to provide safe operating conditions for the transistors. This loop is founded on measurements of DC-link voltage V_{DC} and flying capacitor voltages V_{FC}. As the system is three-level, the voltage of the flying capacitor has to be equal to half of V_{DC}. Later, these two values are compared and given to the FC voltage balancing controller, which results in a value of d_{FC}. Finally, the sum of d and d_{FC} is used for a conventional PWM modulator, thus generating the control signals S_A for transistors $S_{1A\text{-}4A}$.

Note that the control strategy is depicted for one phase only (leg A). However, the control for the second phase is analogous and requires an additional FC voltage balancing controller and an inductor controller current controller (for capacitor C_{FB} voltage balancing and i_{LB} current controlling, respectively).

Unfortunately, due to the unavailability of the researcher from Ukraine, the MPPT algorithm was not developed and is not applied in the built prototype of the interleaved FC DC/DC converter. However, this topic is planned to be investigated in the future.

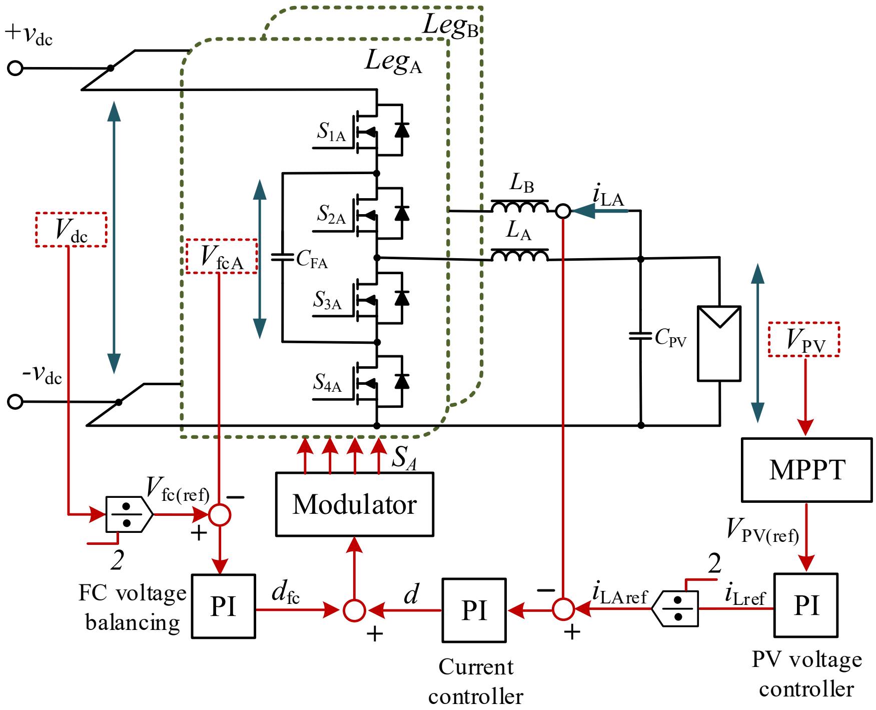

Fig. 3 Control strategy of the interleaved FC DC/DC converter depicted for one phase only (leg A). Second phase is analogous and requires an additional FC voltage balancing controller and a current controller.

2.3 Simulation research

Subsequently, the established topology of the unidirectional DC/DC converter with the developed control algorithm was examined during the simulation study. As in the case of all other converters in the system, the simulations were performed using PLECS software. The built model of the interleaved FC converter was investigated in the full range of V_{PV} voltages and at different power levels. To reach a compromise between power losses and the size of passive components and to sustain a similar value as in other hard-switched converters, the switching frequency f_S was set at the level of 64 kHz. The final values of L_A, L_B, C_{FA}, and C_{FB} to provide the ripples of PV plant current at roughly 20% of the nominal value and flying capacitors voltage below 2% of nominal value was set as 330 μH and 5 μF, respectively. The simulation study confirmed the noteworthy properties of the chosen topology in such applications. The exemplary waveforms recorded in the simulations at a nominal power of 10 kW are presented in Figure 4. As can be seen, due to the interleaved structure, the current drawn from the PV plant is characterized by very low ripples. Moreover, at V_{PV} voltage equal to 800 V, the investigated converter is able to deliver 10 kW to DC-link at the level of 1.5 kV.

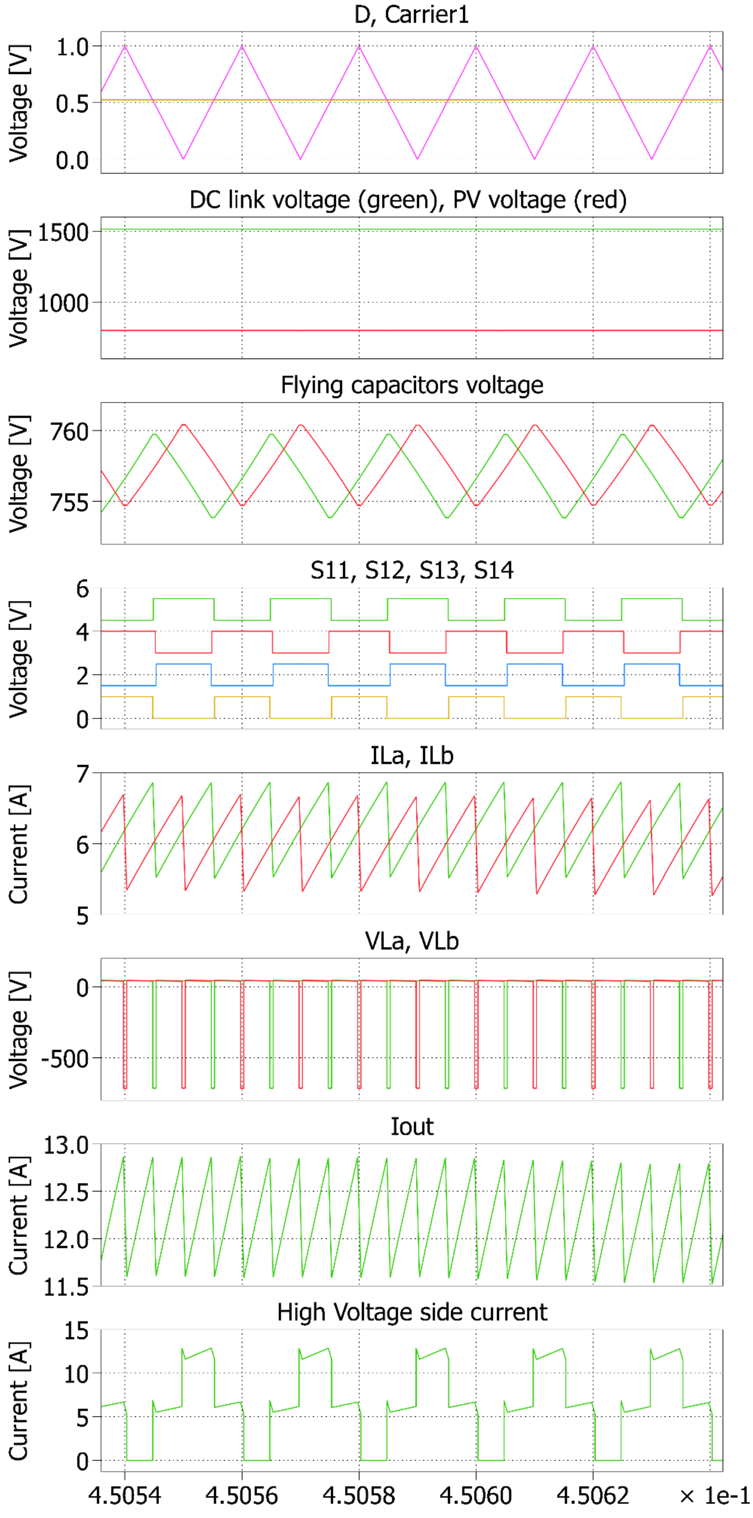

Fig. 4 Simulation waveforms of interleaved FC DC/DC converter at nominal power, 1500 V Dc-link voltage and 800 V PV voltage.

2.4 Hardware prototype

After positive validation of the selected topology of the DC/DC converter and its control algorithm in the simulations, based on the design experience of all previous converters in the system, the laboratory prototype of the interleaved FC DC/DC converter was built. As L_A and L_B inductors the DEMS-65X54/0,33/26 from Feryster were utilized, while as the C_{FA} and C_{FB} WIMA capacitors from snubber MKP series were used. The aim was to employ as many parts of the other converters as possible. Therefore, all gate driver boards, measuring boards, power boards, and control boards were the same as for the non-isolated DC/DC converter interfacing ES with the system. However, the submodule for the interleaved FC converter had to be slightly modified in comparison to the design described in Deliverable D2.1, e.g., to include the flying capacitors. The interleaved FC DC/DC converter enclosed in standard 3U rack housing is depicted in the photograph in Figure 6. All main parameters of the built prototype are listed in Table 1.

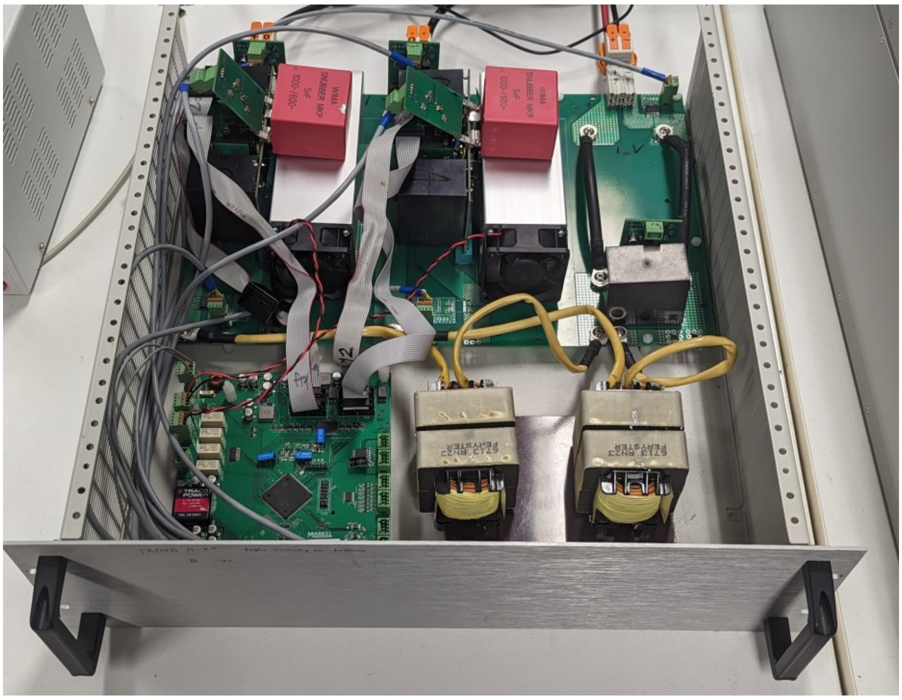

Fig. 6 Prototype of the interleaved FC DC/DC PV converter.

Tab. 1 Parameters of the interleaved FC DC/DC converter

Parameter	Value	Unit
input voltage V_{PV}	300 - 800	V
output voltage V_{DC}	1200 - 1500	V
switching frequency f_S	64	kHz
nominal power P	10	kW
inductors L_A, L_B	330	µH
capacitors C_{FA}, C_{FB}	5	µF
transistors $S_{1A} \div S_{4A}$, $S_{1B} \div S_{4B}$	NTH4L040N120SC1	-

2.5 Experimental verification

Finally, the built prototype was subject to a series of experimental tests at different operating points. The experimental research confirmed the proper operation of the DC/DC converter interfacing PV plant to the advanced EV charging system in the assumed operating range. The exemplary waveforms recorded during experimental tests at nominal power are depicted in Figure 7. The presented waveforms are akin to the results shown in Figure 4 based on simulations, which confirms the proper design of the built prototype. Additionally, to assess the efficiency of energy conversion of the built prototype, the efficiency characteristics were measured for variable P and constant V_{PV} voltage, as presented in Figure 8, as well as for variable V_{PV} and constant P – see Figure 9. The built converter is characterized by decent energy conversion efficiency in almost the entire operating range. The peak recorded efficiency was equal to 98.7% for the nominal voltage of 800 V and a nominal power of 10 kW.

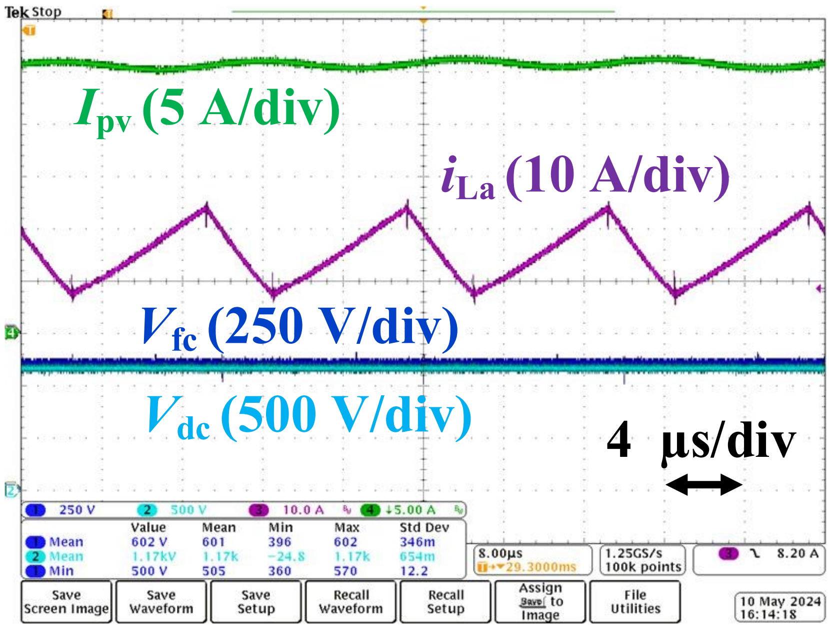

Fig. 7 Exemplary experimental waveforms of the interleaved FC DC/DC PV converter at nominal power of 10 kW, DC-link voltage at 1200 V, and PV voltage at 800 V.

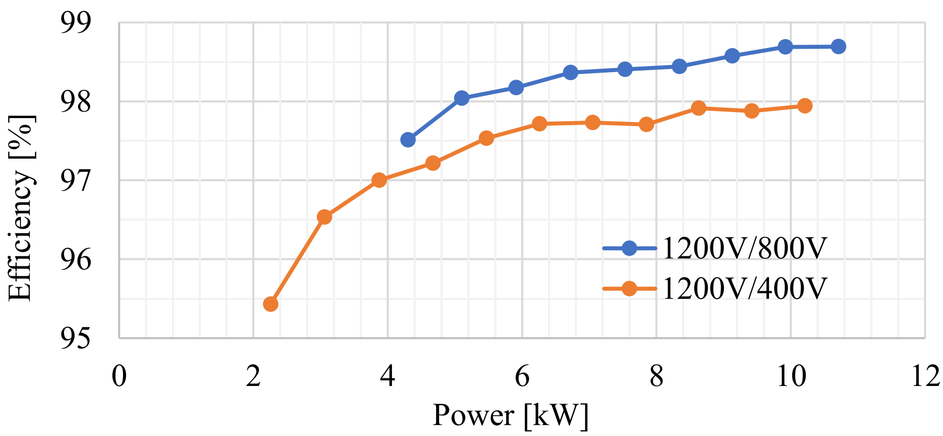

Fig. 8 Efficiency of the interleaved FC DC/DC converter measured for constant voltage of V_{PV} = 800 and 400 V.

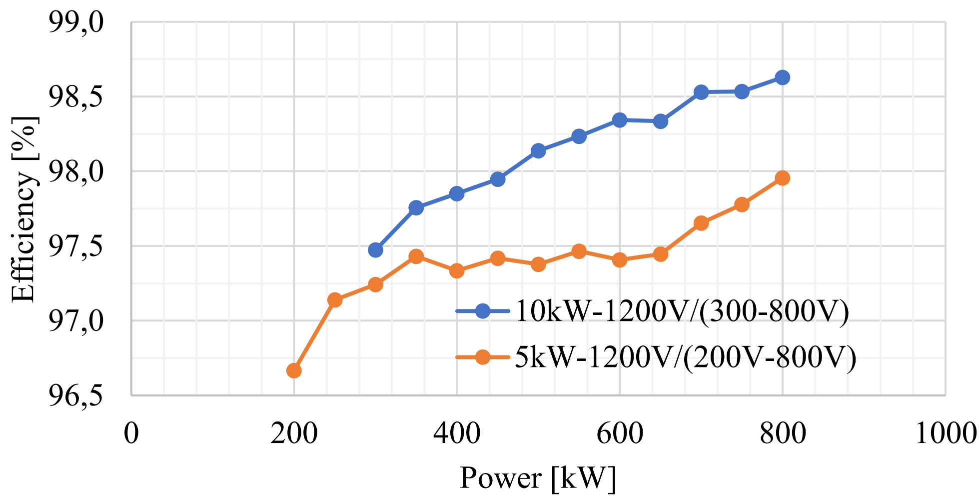

Fig. 9 Efficiency of the interleaved FC DC/DC converter measured for constant power of P = 10 kW and 5 kW.

2.6 Summary

The design process of the DC/DC converter interfacing PV plant to the advanced EV charging system was presented in section 2 of this report. To meet all the requirements for the mentioned converter, a unidirectional, three-level, non-isolated, interleaved FC topology was selected. The simulation research, supported by experimental tests, confirmed the proper selection of topology and control algorithm, enabling the operation of the mentioned converter with good efficiency and connecting the DC/DC converter to the EV charging station. All waveforms recorded in simulations and experiments are convergent, which validates the design of the converter. Moreover, the interleaved FC converter was built based on the existing SiC-based three-level submodule and other converters from the MoReSiC system. The peak measured efficiency for the built prototype of an interleaved FC DC/DC converter was as high as 98.7%. The built model of the mentioned DC/DC converter could be successfully integrated with existing infrastructure in the MoReSiC project to include renewables in the advanced charging station. Due to the serious delay and problematic cooperation with the Ukrainian side, the MPPT algorithm was not implemented into the experimental model. Nevertheless, the rest of the objectives related to the design and experimental verification of the converter enabling connection of the PV plant to the advanced EV charging station have been achieved. Moreover, the analysis of the impact of the PV system on the EV charging station and proposal of PV integration with the rest of the system is included in Deliverable D1.1, while the set of experimental tests with the existing EV charging system has been covered in Deliverable D6.2.

3. Complete integrated advanced EV charging system

After building the required converters in the system, including an additional DC/DC converter to enhance the advanced EV charging system by a PV plant, and their successful experimental validation, all converters have been integrated into the complete EV charging system. Its block diagram is presented in Figure 10, while the photo of the built, advanced EV charging station is depicted in Figure 11. As can be seen in Figure 10, all converters have been connected through a common, three-wire DC-link. From the grid side, the ANPC converter is directly connected to the 3x400 V, 50 Hz grid. Unfortunately, the PV plant, the energy storage, and the electric vehicles were not available during the system's laboratory tests. Therefore, to emulate such loads/sources, adequate power supplies/electronic loads were connected to the converters. The power flow controller implemented on the Raspberry PI was also included in the built system to select the proper operation mode in different situations, according to the energy management algorithm from WP1. Finally, having the entire system connected, the set of experimental tests has been conducted as described in Deliverable D6.2 using proper measuring equipment. Each part of the complete integrated advanced EV charging system is thoroughly described in the following subsections.

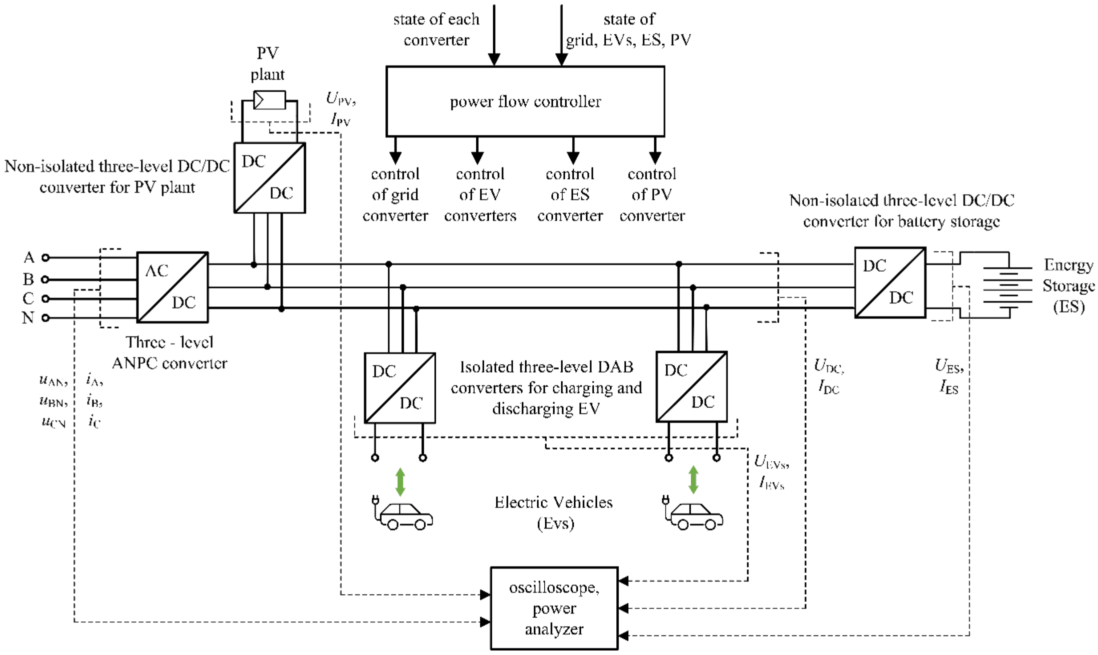

Fig.10 The block diagram of the complete integrated advanced EV charging system .

3.1 The cabinet with all converters

For the convenience of the performed experimental tests, all built converters have been mounted in one rack standard cabinet. The photo of the mentioned cabinet from Base Link is presented in Figure 11. The visible cabinet has the subsequent dimensions: 0.8x1.0x2.055 m. From the top, the control panel is visible, which enables handy control of the charging system and the emulation of various operating modes. Moreover, the control panel is equipped with a dedicated view to observe the status of the charging station and particular converters. From the top, the following converters are mounted: the DC/DC converter for the PV plant, two DC/DC converters for charging and discharging EVs, the DC/DC converter for battery storage, and finally, the AC/DC grid converter. Each converter in the system is connected to the common, medium voltage, and three-wire DC-link. Moreover, for safety reasons, the DC-link could be quickly discharged through a power resistor and manually controlled IGBT transistor. On the left side of the cabinet, the safety button is mounted, which can turn off the entire charging station in case of emergency, bypassing all other protection circuits.

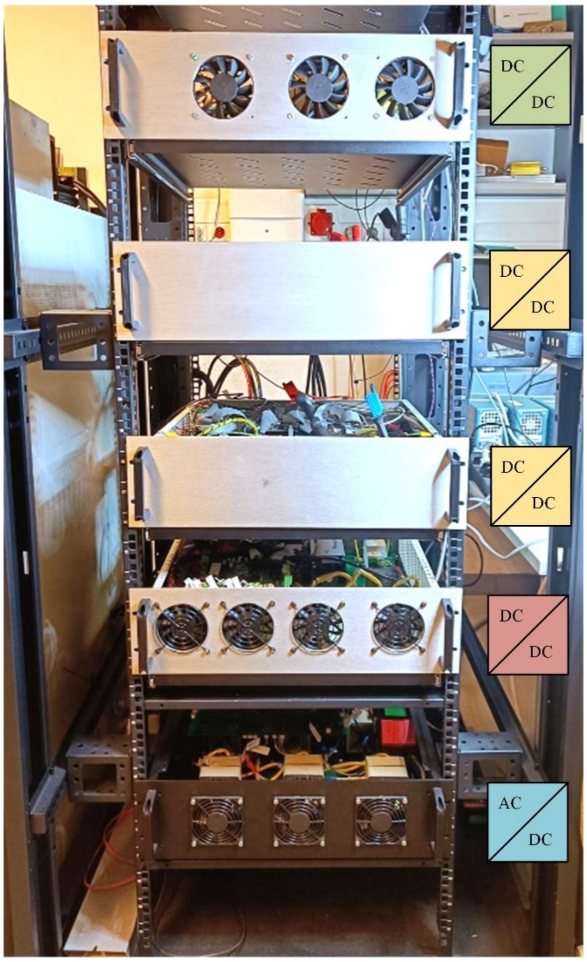

Fig.11 The advanced EV charging system mounted in the rack standard cabinet.

3.2 Power flow controller board

The power flow controller, deciding which operation mode will be optimal under given conditions, was implemented on Raspberry PI model 4B. The photo of the evaluation board with the power flow controller implemented is depicted in Figure 12. To communicate with all converters in the system as well as with the control panel, the power flow controller utilizes a dedicated communication protocol using the CAN standard. Through the proper design of the communication network inside the rack cabinet with mounted converters, the communication system is immune to EMI emitted in the system and enables the safe operation of the entire system. The power flow controller allows to set the reference values in the test operating mode and also provides the ability to control the system's operating status. Through dedicated software created for the project, it is also possible to read the parameters of the entire charging system, such as voltages, currents, and temperatures.

a)

b)

Fig.12 The power flow controller: a) Raspberry PI 4B evaluation board, b) a photograph of the screen with the user interface.

3.3 Emulation of PV plant, EV and ES

As mentioned earlier, it was not possible to connect the PV plant, the energy storage, and the electric vehicles to the built system during laboratory tests. Nevertheless, to emulate such loads/sources, it was decided to use unidirectional and bidirectional power supplies from Elektro-Automatik EA-PSB and EA-PSBE series, which provide the same operating conditions for the converters as the real loads would. The photo of the cabinet with the mentioned power supplies is presented in Figure 13. The unidirectional power supply was connected from the PV plant side, while the bidirectional power supplies were connected from the EVs and ES sides. In that way, when charging the EVs or ES, the energy was returned to the grid. One of the main advantages of such an approach is that the necessary power to conduct such tests is equal to only the power losses of particular converters.

Fig.13 The photo of the cabinet with power supplies emulating PV, EVs and ES.

3.4 Measuring setup

To observe the waveforms in the advanced EV charging system as well as to assess the parameters of the energy conversion, precise laboratory equipment is necessary. To fulfill this requirement, the following measuring devices were used: oscilloscope MSO56 series 5 from Tektronix, power analyzer Yokogawa WT1800 and WT5000, high voltage differential probes THDP0100 and THDP0200 from Tektronix, current probes TCP404XL and TCP0030A. Utilizing such specialized equipment, it was certain that the results obtained were consistent with the actual waveforms and parameters in the system.

4. Conclusion

In the presented report, the complete integrated advanced EV charging system was presented. The system consists of a 20 kVA multilevel AC-DC converter, two 10 kW isolated DC-DC converters, and a 20 kW non-isolated DC-DC converter under the control of the power flow controller. The integration of the mentioned converters into one properly operating, advanced EV charging system was the main objective of Deliverable D6.1, which was covered by task T6.1 in WP6. As presented above, this target was fulfilled. Moreover, based on the Annex MoReSiC-UA titled "Photovoltaic Extension for Bidirectional Charging Infrastructure for Electric Vehicles," the system was extended by an interleaved FC DC/DC converter integrating a PV plant into the system. The design process of the mentioned converter, including the selection of topology, control algorithm, simulation tests, hardware prototype, and experimental validation, is included in section 2 of this report. The additional converter was successfully integrated with the previously existing system and operated with the power flow controller. The complete integrated EV charging system, which is the subject of this report, was used to conduct the series of experimental tests presented in Deliverable D6.2.